Revealing the Recent Height Changes of the Great Altesch Glacier Using TanDEM-X DEM Series

Master Thesis

Author(s):
Vlieghe, Pierre-Louis

Publication date:
2023-10

Permanent link:
https://doi.org/10.3929/ethz-b-000637956

ETH
Eidgenössische Technische Hochschule Zürich
Swiss Federal Institute of Technology Zurich

Earth Observation and Remote Sensing

Pierre-Louis Vlieghe

Revealing the Recent Height Changes of the Great Altesch Glacier Using TanDEM-X DEM Series

Master Thesis

Institute of Environmental Engineering
Swiss Federal Institute of Technology (ETH) Zurich

Supervision

Shiyi Li
Prof. Dr. Irena Hajnsek

October 2023

Contents

Abstract

Monitoring glacier mass balance is essential for understanding glacier-climate interactions and predicting water resources management. As the largest glacier in the Alps, the Great Aletsch Glacier has a length of 22 km and covers about of 78 km^2 [4]. It contains 20% of the entire Swiss ice mass [4], and thus plays significent role in understanding the dynamics of glacier mass change in this region. Because of its significance, the TanDEM-X satellite mission has selected the Great Aletsch Glacier as a super-testsite and has collected abundant single-pass bistatic Synthtetic Aperture Radar (SAR) data over the glacier since 2011. Leveraging these TanDEM-X satellite data, we generated 124 digital elevation models (DEMs) from the Coregistered Single-look Slant Range Complex (CoSSC) data product, calculated glacier elevation changes between 2011 and 2022, and quantified the temporal dynamics of the mass balance of the Great Aletsch Glacier.

The DEMs were generated using an iterative approach. We initially used an external DEM (swissALTI3D [10]) as the reference for geocoding and interferogram simulation. The simulated interferogram was subtracted from the interferogram between the CoSSC data pairs to generated a differential interferogram. The unwrapped phase in the differential interferogram corresponds to the height difference between the TanDEM-X measurements and the reference DEM, and thus we converted the phase into differential height to update the reference DEM. At this point, the updated reference DEM was accepted as the final product if the mean and standard deviation of the differential height met with the convergence criteria, otherwise it was used as the new reference in the subsequent iteration.

Following the DEM generation, we used xDEM python package [5] to analyze the DEM series. We first measured the elevation change by differencing two DEMs, then used a local hypsometric interpolation method to fill the dDEM voids within the glacier outline, and finally integrated the elevation difference over the glacier to calculate the ice volume and mass change. Our results revealed a consistent glacier-wide height loss of 1 $\mathrm{m\,a^{-1}}$ on average between 2011 and 2022, corresponding to a cumulative volumetric ice loss of 79×10^6 $\mathrm{m^3\,a^{-1}}$ and mass loss of 68 $\mathrm{Mt\,a^{-1}}$ (assuming a mean ice density of 850 $\mathrm{kg\,m^3}$ [7]). Notably, the Konkordiaplatz region, situated at elevations between 2600 and 2800 meters, exhibited an average elevation loss of 2.3 $\mathrm{m\,a^{-1}}$, whereas the Glacier tongue region, ranging in elevation between 1900 and 2100 meters, witnessed an average elevation loss of 5.2 $\mathrm{m\,a^{-1}}$.

In summary, our results have provided valuable insights into the dynamic changes of the Great Aletsch Glacier by analyzing the abundant TanDEM-X data. The detailed spatiotemporal of our work advanced our understanding of glacier recession in the Alps under the climate change.

Acknowledgment

I would like to express my deep gratitude to all the members of the Earth Observation group who have warmly welcomed me and shared the exciting adventure of my Master's thesis over the past six months.
In particular, I wish to express my profound appreciation to my supervisor, Shiyi Li, whose guidance and support have been instrumental in developing my understanding and knowledge in a field that was uncharted territory for me.
I would also like to thank Irena Hajnsek for giving me the opportunity to delve into this subject and placed her trust in me.
To each member of the Earth Observation group, thank you for your contributions that have enriched my learning experienced. This Master's thesis has been a remarkable chapter in my academic journey, and I am very proud to have worked alongside you in the exciting field of Earth Observation and Remote Sensing.

Nomenclature

Acronyms and Abbreviations

CoSSC	Coregistered Single look Slant range Complex
CRS	Coordinate Reference System
deg	Degree
dDEM	Digital Elevation Model Difference
DEM	Digital Elevation Model
ETH	Eidgenössische Technische Hochschule
ETRS89	European Terrestrial Reference System 1989
GLAMOS	Glacier Monitoring Switzerland
GPS	Global Positioning System
HH	Horizontal transmit, Horizontal receive
HOA	Height of Ambiguity
InSAR	Interferometric Synthetic-Aperture Radar
LN02	Swiss national levelling network
m a.e	Ellipsoid heights (meters above ellipsoid)
m a.s.l	meters above sea level
MCF	Minimum-Cost Flow
RMSE	Root Mean Square Error
R^2	Coefficient of determination
SAR	Synthetic-Aperture Radar
VAW	Versuchsanstalt fur Wasserbau, Hydrologie und Glaziologie
VV	Vertical transmit, Vertical receive
WGS84	World Geodetic System 1984

Chapter 1

Introduction

Glaciers are pivotal components in the Earth's climate system, serving as sensitive indicators of climatic variations at both regional and global scales. Their dynamic behavior offers valuable insights into the intricate processes governing our planet. These massive ice masses significantly influence hydrological, geological, and ecological systems, contributing to the complex web of natural processes [8]. Therefore, it is crucial to monitor their height changes and to quantify their mass balance accurately.
Among the glaciers of the world, the Great Aletsch Glacier stands out for its size and significance. Located in the heart of the Alps, it is the largest glacier in the region, covering an area of 78 km^2 and accounting for about 20% of Switzerland's ice volume. Its dimensions include a length of 22 km, a mean thickness of 147 m, and a volume of 11 km^3 [3]. Due to its importance in cryospheric research, the TanDEM-X mission has designated it as one of its two alpine super-test sites, along with the Columbia Glacier in Alaska [17].
The TanDEM-X mission uses the Synthetic Aperture Radar (SAR) technology that have the advantage of being able to image snow and glaciers regardless of weather and daylight conditions with some drawbacks, such as the penetration of microwaves into dry snow, which reduces the accuracy of the DEMs, and the limited coverage of the scene due to radar shadow and layover in rugged terrain. The main goal of this mission is to produce a high precision DEM that covers 97% of the land surface on Earth [12]. The TanDEM-X mission has imaged the Aletsch Glacier from the same orbit using a series of about 130 bistatic stripmap scenes with different across-track baselines. Thanks to the TanDEM-X data product we can generate per-scene DEMs by using the coregistered single look slant range complex pairs (CoSSC specification [15] and [13]), which are the basis for InSAR processing.
This study aims to comprehensively investigate the dynamics height changes of the Great Aletsch Glacier, utilizing Digital Elevation Models (DEMs) derived from TanDEM-X data series. The study seeks to answer the following research questions:

- What is the spatial distribution of height changes across the Great Aletsch Glacier over the past decade?
- How has the cumulative height and mass change of the Great Aletsch Glacier evolved from 2011 to 2022?
- What are the trends in mean annual height changes in different zones of the Great Aletsch Glacier?

This thesis follows a structured approach, with the subsequent section providing an overview of the study area and the dataset, encompassing TanDEM-X data, GPS measurements, and external DEMs. The methodology section delves into InSAR DEM generation and Digital Elevation Model differences (dDEMs). The results section presents findings, including DEM validation and comparison through field measurements, the glacier's height evolution over the specified time frame, and comparisons between distinct periods (2011-2016 and 2017-2022).

Chapter 2

Study Area and Dataset

2.1 The Great Aletsch Glacier

The Great Aletsch Glacier stands as one of the most iconic and significant glaciers within the European Alps. Located in the heart of the Swiss Alps, the glacier is nestled within the Bernese Oberland region, specifically within the canton of Valais [16]. Its vast expanse and unique characteristics make it a prominent subject of study in the field of glaciology and climatology, attracting researchers and enthusiasts from around the world. This immense glacier begins its journey from the prominent Jungfrau Massif and the Aletschhorn, both towering peaks that reach altitudes of over 4000 meters. From these high alpine regions, the glacier descends through a series of valleys, ultimately terminating at an elevation of approximately 2000 meters above sea level.

2.1.1 The Glacier Outline

The glacier outline used in this study for the Great Aletsch Glacier, delineated in black in Figure 2.1, is derived from the Swiss Glacier Inventory 2016 [2], which provides glacier outlines and related data for the period 2013-2018. This dataset is based on aerial imagery and stereophotogrammetric analysis conducted by the Swiss Federal Office of Topography (swisstopo) as part of the Topographic Landscape Model of Switzerland (swissTLM3D). It has been rigorously revised by glaciologists from VAW-ETH Zurich, the University of Zurich, and the University of Fribourg. Refer to the table in the Appendix A.1 for a comprehensive summary of the key characteristics of the glacier outline (area, elevation range, average slope, and average aspect). This glacier outline which represent the Aletsch glacier outline in 2017 forms the basis for our analysis and interpretations in this study.

2.2 The Konkordiaplatz and the Glacier Tongue Region

These areas, illustrated in blue in Figure 2.1, serve as focal points for the analysis of glacier elevation change time series. The key characteristics such as area, elevation range, average slope, and average aspect for this region are available in the Appendix A.2.

2.2.1 The Konkordiaplatz

The Konkordiaplatz is a distinctive geographical area situated just south of the Jungfrau in the Great Altesch Glacier. This flat area, with a surface area of 7.38 km^2, is characterized

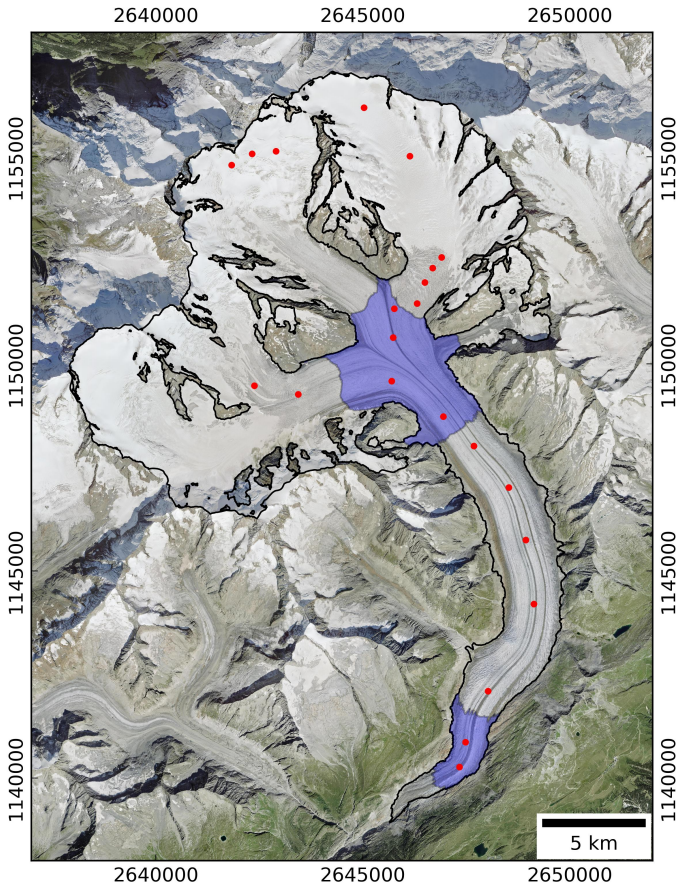

Figure 2.1: Overview of the study area: the Great Aletsch Glacier. The glacier outline is delineated in black according to GLAMOS [2], with the enclosed area serving as the spatial coverage for analysis. Two specific regions of interest are highlighted in blue Konkordiaplatz at the top (2600-2800 m above ellipsoid) and the glacier's tongue at the bottom (1900-2100 m above ellipsoid). Red dots mark the locations of GPS measurements. The base image used in this representation is sourced from SWISSIMAGE 25, 2017-2019, swisstopo (JD100042). Swiss reference system: CH1903+.

by a vast expanse of snow and ice. It holds unique significance due to its position as the confluence point of four major glaciers: the Aletschfirn, Jungfraufirn, Ewigschneefäld, and Grüneggfirn. The Konkordiaplatz blue region in Figure 2.1 has been defined between two level lines, 2600 and 2800 meters above ellipsoid, within the glacier outline.

2.2.2 The Glacier Tongue

The second region of interest within our study is the glacier tongue. The glacier tongue represents the lowermost section of the glacier and exhibits dynamic responses to environmental changes, including climate fluctuations. For our study, we specifically selected a glacier tongue region with a surface area of 1.63 km^2, situated between the two level lines at 1900 and 2100 meters above ellipsoid. This choice was made to avoid areas where the glacier has receded beyond 1600 meters, ensuring that we focus on a region where ice is consistently present throughout the observed time period from 2011 to 2022.

2.3 TanDEM-X Data

The dataset encompasses 124 bistatic, dual-polarization TanDEM-X stripmap acquisitions. These acquisitions were consistently obtained from orbit 154, adopting a descending imaging configuration, with a westward orientation and an approximate incidence angle of 32 degrees. In order to explore various bistatic configurations, the effective perpendicular baselines, responsible for determining the height of ambiguity for across-track interferometry, generally ranged from 0 to 200 meters. However, during the extensive baseline acquisition period in spring 2015, these baselines were extended to as much as 1040 meters. To maintain data consistency, our dataset selection criteria included data with a height of ambiguity falling within the range of 15 to 600 meters. Refer to the Appendix A.3 to find the TanDEM-X data specification of our dataset.

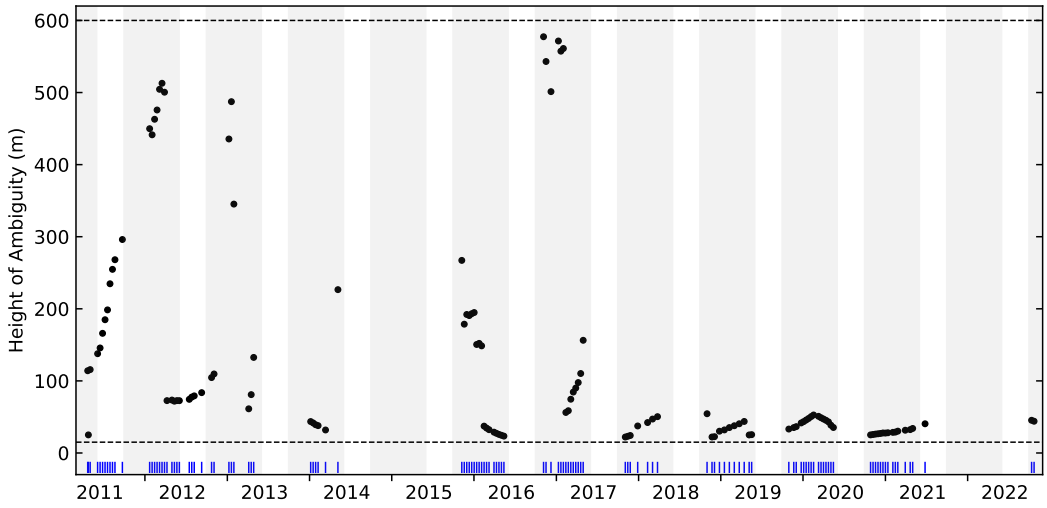

Figure 2.2: Height of ambiguity within the dataset, with temporal distribution of data acquisitions. The gray shaded region highlights the majority of data collected between 1st October and 31th May (winter season), while data from the summer months of 2011 and 2012 are also included. Horizontal dashed lines at 15 and 600 meters mark the threshold for the height of ambiguity. Blue ticks along the timeline provide a visual representation of the temporal spacing between data acquisitions.

All of the acquired data were captured in two polarizations: HH and VV polarization. However we only use the data in HH polarization. In slant range and azimuth the spatial resolution was set with a pixel spacing of 1.75 x 2.3 meters on the horizontal ground. TanDEM-X follows an orbit repeat interval of 11 days. However, due to competing priorities and constraints, acquisitions could not be obtained during every orbit pass. Consequently, the resulting time series exhibits gaps at intervals that are multiples of 11 days. For a comprehensive overview of acquisition dates, refer to the blue tick marks in Figure 2.2. Given that the area primarily serves as a snow-specific super test site, the majority of acquisitions are available during the winter seasons between the months of October and May. Nevertheless, a limited number of acquisitions were recorded during the summer seasons of 2011 and 2012, and due to the height of ambiguity criteria we do not have TanDEM-X data for winter 2014-2015 and winter 2021-2022.

2.4 Field Measurements for Validation

In order to validate the accuracy and reliability of our DEMs presented in this study, we used GPS field measurements conducted on April 30/May 01, 2019 by Sylvain Leinss and Philipp Bernhard and described in their article [9]. The field campaigns were carried out at 22 specific locations, as indicated by red dots in Figure 2.1. At each measurement location, they meticulously recorded the position using geodetic GPS equipment. They placed 140 cm long bamboo sticks in the snow and measured the position with a geodetic GPS. The accuracy of about 2-3 cm was limited by the diameter of the sticks. A summary of the collected data, including coordinates, measurement dates, and ellipsoid height, is presented in Table 2.1.

Point	Longitude (deg)	Latitude (deg)	Ellipsoid height (m)	GPS start time
P00	7.98401	46.5432	3392.25	2019-04-30
P01	7.99050	46.5456	3495.35	2019-04-30
P02	7.99800	46.5461	3504.58	2019-04-30
P03	8.02580	46.5554	3466.93	2019-04-30
P04	8.04018	46.5448	3361.51	2019-04-30
P05	8.04989	46.5228	3167.31	2019-04-30
P06	8.04706	46.5205	3128.02	2019-04-30
P07	8.04458	46.5173	3049.90	2019-04-30
P08	8.04210	46.5128	2864.36	2019-04-30
P09	8.03486	46.5117	2787.53	2019-04-30
P10	8.03441	46.5054	2744.42	2019-05-01
P11	7.99072	46.4952	2977.17	2019-05-01
P12	8.00449	46.4932	2897.60	2019-05-01
P13	8.03385	46.4960	2729.18	2019-05-01
P14	8.05002	46.4882	2639.29	2019-05-01
P15	8.05955	46.4817	2557.53	2019-05-01
P16	8.07048	46.4726	2483.36	2019-05-01
P17	8.07570	46.4612	2431.50	2019-05-01
P18	8.07806	46.4473	2341.23	2019-05-01
P19	8.06338	46.4285	2141.57	2019-05-01
P20	8.05620	46.4174	2055.19	2019-05-01
P21	8.05424	46.4121	1973.13	2019-05-01

Table 2.1: GPS Data Information, with the geographic (GPS) coordinates: WGS84, the ellipsoid height and the date of acquisition.

2.5 External DEM

2.5.1 Raster for DEM Height Transformation

In our study, we employed a DEM sourced from Swisstopo: swissALTI3D [10].This DEM uses the official height system Swiss national levelling network (LN02). This system was defined by anchoring the 'height above sea level' to the Repere Pierre du Niton at 373.6 meters in Geneva. However, for the purposes of our study, we needed to convert the swissALTI3D DEM from the LN02 system to ellipsoid height, a necessary step for DEM generation. To accomplish this transformation, we relied on a Geotiff raster that provided

the height difference information between the ellipsoid height (ETRS89) and the Swiss national levelling (LN02) heights across Switzerland [1].

2.5.2 SwissALTI3D DEM

The study area's alpine terrain, ranging from 600 to 4200 meters above sea level, posed challenges for InSAR processing due to steep slopes causing radar layover and shadow issues. To simplify processing, we subtracted a simulated interferogram using the SwissALTI3D Digital Elevation Model from SwissTopo, generated in 2022 with data mainly from 2017 (date of flight) [6]. In ice and snow-free areas, the model offers a vertical precision of 0.5 meters (stereo-correlation) below 2000 meters and 1-3 meters above [11]. We also re-sampled the horizontal resolution from 2 to 10 meters for faster processing.

2.5.3 DEM Generated by a Different Method

The last external DEMs employed serve the purpose of DEM validation. These DEMs utilizes the same TanDEM-X data source but employing a distinct approach for DEM generation. The external DEM generation method entails the utilization of a custom code developed by Sylvain Leinss and Philipp Bernhard. This method circumvents common pitfalls associated with InSAR DEM generation and implements an InSAR-based orthorectification process, all details of the DEM generation method are described the section III of the article [9]. The initial external DEM, dated May 7, 2019, is juxtaposed with our own DEM captured on the same date. This comparison is accompanied by GPS data, as illustrated in Figure 4.1. The selection of this date closely aligns with the acquisition date of the field measurements in the Table 2.1.

Chapter 3

Methods

3.1 Data Preparation and Preprocessing for swissALTI3D DEM

In the initial phase of our study, we obtained highly precise DEM tiles from swissALTI3D to create our reference DEM, which represents the study area. We performed essential data transformations, beginning with the reprojection and downsampling of the merged swissALTI3D DEM to achieve a resolution of 10x10 meters using bilinear interpolation. Subsequently, we transformed the elevation values from LN02 to ellipsoid height by adding the elevation transformation raster to the merged swissALTI3D DEM. Finally, for broader compatibility and international standardization, we reprojected the swissALTI3D DEM into the WGS84 coordinate system.

3.2 Generation of DEMs

In this section, we elucidate the methodology employed for the generation of Digital Elevation Models (DEMs) in the context of our study. The DEMs were created through an iterative process aimed at refining the accuracy and precision of elevation measurements.

3.2.1 Reference DEM and Interferogram Simulation

The initial step in our DEM generation approach involved the utilization of the swissALTI3D DEM as a reference for geocoding and interferogram simulation. Interferogram simulation was carried out using the *phase_sim_orb* function within the GAMMA software [14]. This function facilitated the simulation of the unwrapped phase, utilizing elevation data from the reference DEM and baseline information.

3.2.2 Differential Interferogram Generation

To create the differential interferogram, the simulated interferogram was subtracted from the interferogram acquired from the CoSSC data pairs. We accomplished this using the *SLC_diff_intf* function, also part of the GAMMA software [14]. Notably, the *SLC_diff_intf* function generates the differential interferogram directly from co-registered Single Look Complex (SLC) images, obviating the need for an intermediary interferogram. Furthermore, it applies range-adaptive common band filtering, yielding a wrapped differential

interferogram. This advanced procedure is particularly beneficial when processing interferometric data in areas characterized by hilly or mountainous terrain. It achieves this by leveraging local slope information to mitigate spatial decorrelation induced by non-flat topography.

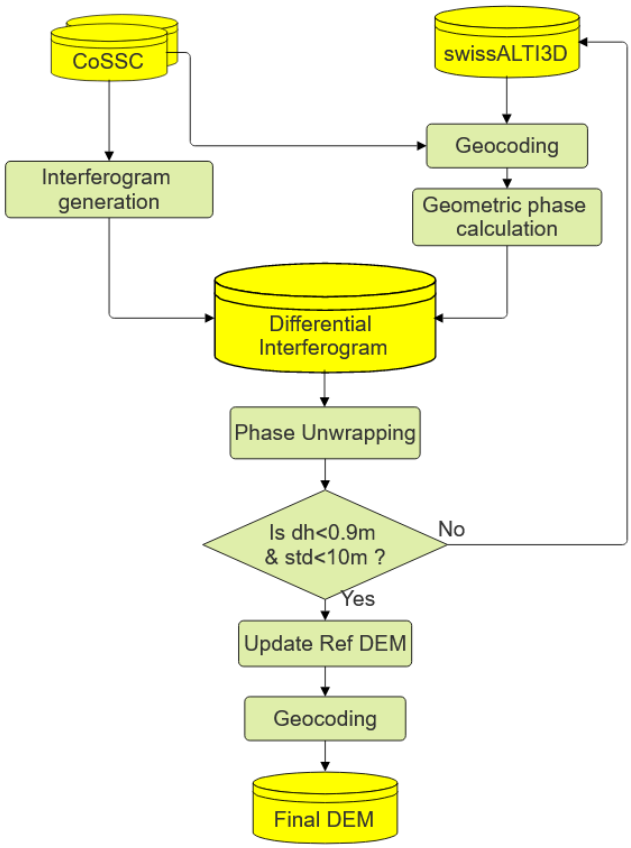

Figure 3.1: DEM generation workflow.

3.2.3 Phase Unwrapping with MCF Algorithm

Subsequent to the generation of the differential interferogram, we employed the Minimum Cost Flow (MCF) algorithm to perform phase unwrapping. This crucial step allowed us to convert the phase information in the differential interferogram into differential height measurements.

3.2.4 Conversion and Convergence Criteria

The unwrapped phase in the differential interferogram inherently corresponds to the height difference between the TanDEM-X measurements and the reference DEM. To ensure the accuracy and reliability of our DEMs, we imposed convergence criteria on the differential height. Specifically, we required that the mean differential height be less than 0.9 meters and the standard deviation be below 10 meters. If these criteria are met, the differential height is added to the reference DEM, and the resulting DEM is transformed into map coordinates.

3.2.5 Iterative Refinement

In cases where the convergence criteria were not met, indicating potential inaccuracies in the interferogram, an iterative process is initiated. The reference DEM is updated by incorporating the differential height, and the InSAR-based height data (in slant-range coordinates) were correctly transformed into map coordinates. This transformation is achieved by updating the orthorectification lookup table using the *gc_ insar* function from the GAMMA software [14]. Subsequently, a new iteration commenced with the refined reference DEM. This iterative approach allowed us to progressively improve the accuracy and precision of the generated DEMs, particularly in areas characterized by challenging topography.

3.3 Digital Elevation Model Difference: dDEM

To understand the spatial distribution and magnitude of elevation change over the glacier, we calculated 124 Digital Elevation Models Difference (dDEMs). A dDEM quantifies elevation changes between two timestamps by subtracting the values of one DEM from another on a pixel-by-pixel basis. The workflow to generate dDEMs can be found in Appendix A.5.

3.3.1 Preprocessing for dDEM Generation

In order to maintain consistency and compatibility among our DEMs, we applied a sequence of preprocessing steps to each DEM. This included reprojecting, resampling, and cropping the DEMs to align with the specifications of our reference DEM swissALTI3D (Refer to the subsection 3.1). We also carefully managed Nodata values by assigning them as None, ensuring consistent calculations in subsequent analyses.

3.3.2 dDEM Generation

For the purpose of examining the time-dependent progression of elevation changes of the glacier, we employed the Python package xdem.DEMCollection. This package enables us to handle multiple timestamps concurrently and simplifies the computation of elevation/volume changes over several years. We utilized the xdem.DEMcollection.subtract_dems() function to create the differential DEMs (dDEMs) by subtracting all DEMs from the oldest DEM, which in our study corresponds to the data collected on April 22, 2011. As a result, each dDEM illustrates the elevation changes relative to this date.

3.3.3 Interpolating Nodata Gaps in the dDEM

To calculate consistent elevation changes across the glacier using our dDEMs, we must address the Nodata gaps within the glacier outline, delineated in black in the Figure 2.1. We employed a xDEM function to perform interpolation within our DEMCollection object. Specifically, we adopted a local hypsometric interpolation method, which capitalizes on the typical relationship between elevation and elevation change in glaciers.
In this glacier-specific approach, the local hypsometric method estimated elevation change gradients for the glacier by creating linear or polynomial models using the dDEM and the reference DEM, which is in our case the swissALTI3D. This model enables us to fill voids within the dDEM by replacing them with expected values based on the elevation,

as predicted by the models. Note that for each dDEM the numbers of pixels interpolated and surface interpolated in percentage for the glacier, Konkordiaplatz and the tongue can be found in the Appendix A.5.

3.4 Calculation of Glacier Mass Balance

In the context of glacier mass balance assessment, differential digital elevation models (dDEMs) are instrumental. These dDEMs allow for precise volume loss determination within the glacier. This involves computing the mean height loss across the glacier, using the dDEMs, with consideration of a glacier outline delineated in Figure 2.1 that confines the analysis to the glacier's extent. This mean height loss is then multiplied by the glacier's surface area defined by the glacier outline, yielding the volume loss. Finally, the mass balance is obtained by multiplying the volume loss by this density, assuming an ice density of $850\,\mathrm{kg\,m^{-3}}$ [7].

Chapter 4

Results

4.1 Validation and Comparison of DEMs

In this section 4.1, both DEMs use TanDEM-X data dated May 7, 2019: one generated using our method and the other using an alternative approach described in Subsection 2.5.3. The assessment is based on a comparison with ground truth data obtained from GPS measurements described in Section 2.4, which serves as a reliable reference for elevation values.

4.1.1 DEMs Versus GPS Measurements

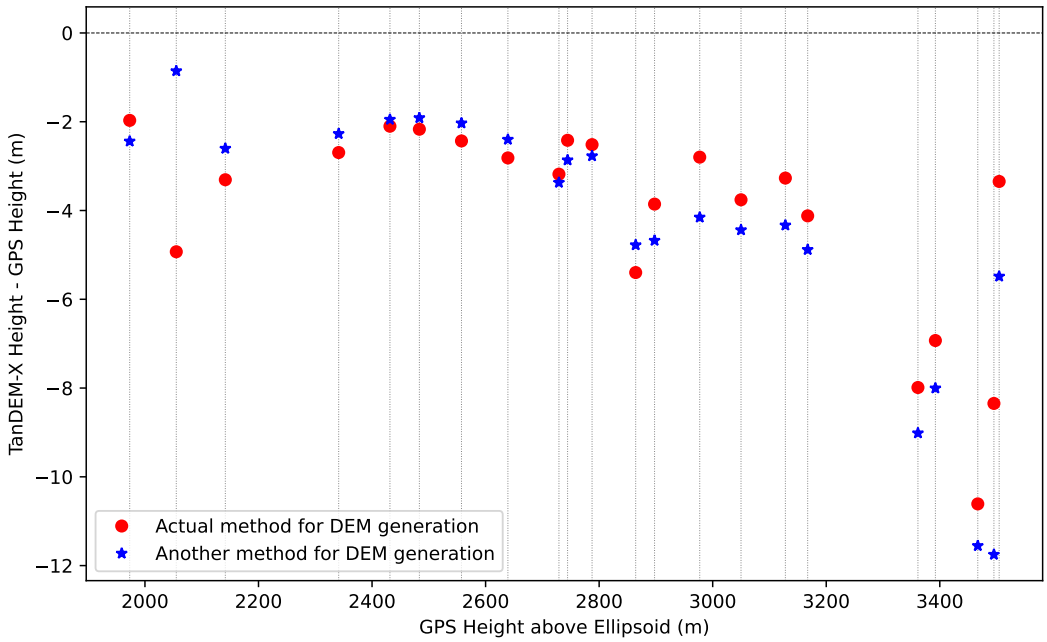

Figure 4.1: Validation and Comparison of DEM Accuracy: Red dots represent the height differences between TanDEM-X and GPS measurements for the DEM generated with our method described in Section 3.2. Blue stars represent the height differences for an external DEM generated using a different method described in Subsection 2.5.3.

The first Figure 4.1 shows the comparison between TanDEM-X heights and GPS-measured heights. It is evident from this figure that the TanDEM-X heights consistently underestimate the GPS heights by several meters. The root mean square error (RMSE) between TanDEM-X heights and field measurements is calculated to be 4.7 meters for our method and 5.4 meters for the alternative method. This underestimation is more pronounced at higher elevations above Konkordiaplatz, where the TanDEM-X heights are up to 11 meters below the GPS measurements.

4.1.2 DEM Versus DEM Generated by a Different Method

As we move beyond an elevation of 2900 meters in Figure 4.1, the DEM generated using our method exhibits closer agreement with the GPS heights in comparison to the DEM generated using the alternative method. To illustrate this, Figure 4.2 displays a map that depicts the pixelwise differences in elevation between the two DEMs.

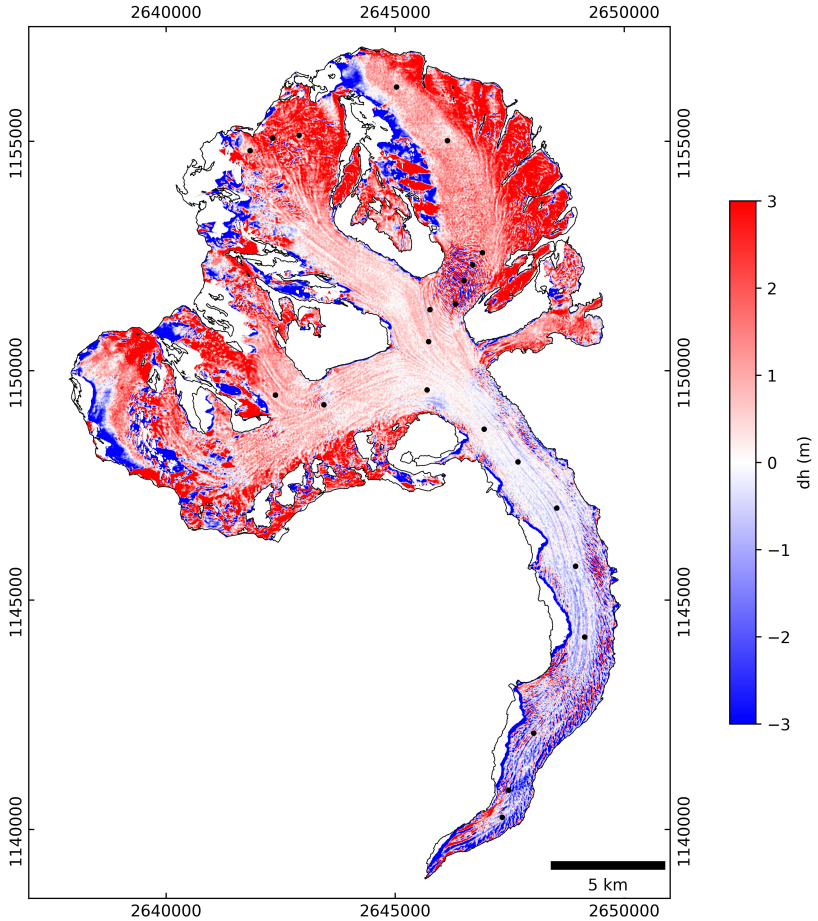

Figure 4.2: DEMs difference: DEM generated with our method minus DEM generated with another method described in Subsection 2.5.3. Both DEMs were generated using TanDEM-X data dated May 7, 2019. Pixel-by-pixel difference within the glacier outline delineated by the black outline, no interpolation was applied and the DEM generated by the other method was coregistered. Black dots indicate the 22 GPS measurements. Blue represents negative elevation differences, while red signifies a positive one. Swiss reference system: CH1903+.

The mean difference across all pixels is calculated to be 0.52 meters, with a standard deviation of 3.13 meters. This map reveals spatial patterns in the discrepancies between the two DEMs. We observe that in regions characterized by complex topography with steep slopes, such as the edges of the glacier, the differences between the two DEMs are more substantial. In contrast, in flatter areas like Konkordiaplatz, the differences are negligible, averaging around 0 meters. Notably, above Konkordiaplatz, the difference in elevation is positive (colored red), indicating that our method experiences less penetration, while below Konkordiaplatz, the differences tend to be more negative (colored blue) with sporadic red zones.

4.2 Elevation Loss

4.2.1 Cumulative Height and Mass Loss

For the Aletsch Glacier, from April 22, 2011, to October 23, 2022, we observed in Figure 4.3 a cumulative height loss of -14 meters and a cumulative mass loss of -940 Mt. The linear regression fit yielded a slope coefficient of$-1\ \mathrm{m\,a^{-1}}$, equivalent to an annual mass loss of approximately $-68\ \mathrm{Mt\,a^{-1}}$, with a coefficient of determination (R^2) of 0.91.

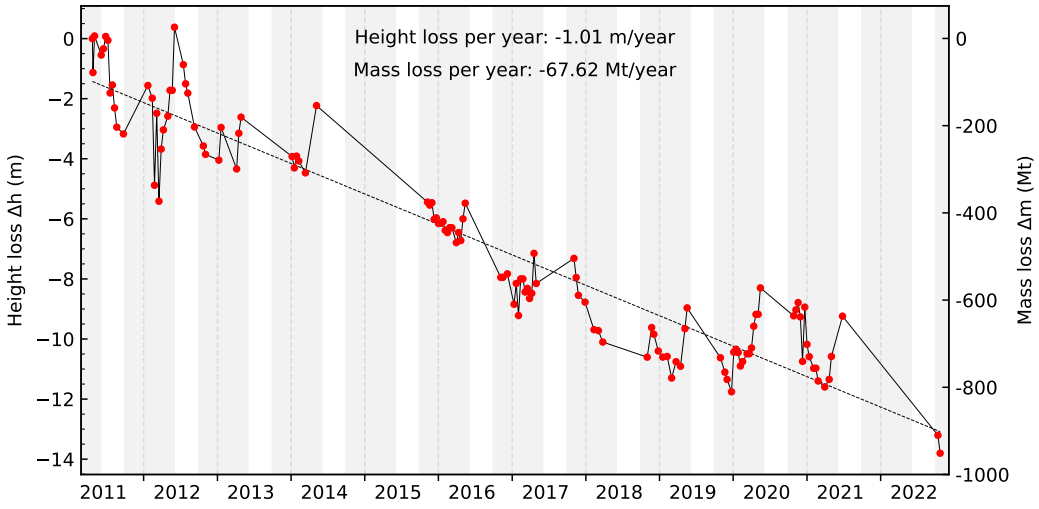

Figure 4.3: Cumulative average height and mass loss over time (2011-2022): Left y-axis shows the cumulative average height loss relative to the initial measurement on April 22, 2011. The right y-axis corresponds to cumulative average mass loss derived from height loss (see Section 3.4). The plot includes 124 red dots, representing cumulative height/mass loss at every timestamps between 2011 and 2022. The gray shaded region highlights the winter season from October 1 to May 31. A dashed line indicates the linear regression fit, with the slope coefficient providing the annual height/mass loss rate.

For the two other zones, Figure 4.4 shows the cumulative height loss. At Konkordiaplatz, within the elevation range of 2600 to 2800 meters, the cumulative height loss was -30 meters, with a rate of height loss of $-2.3\ \mathrm{m\,a^{-1}}$($R^2 = 0.97$). In the glacier tongue zone, 500 meters below, between elevations of 1900 to 2100 meters, the cumulative height loss was -71 meters, with a rate of $-5.2\ \mathrm{m\,a^{-1}}$ ($R^2 = 0.96$).

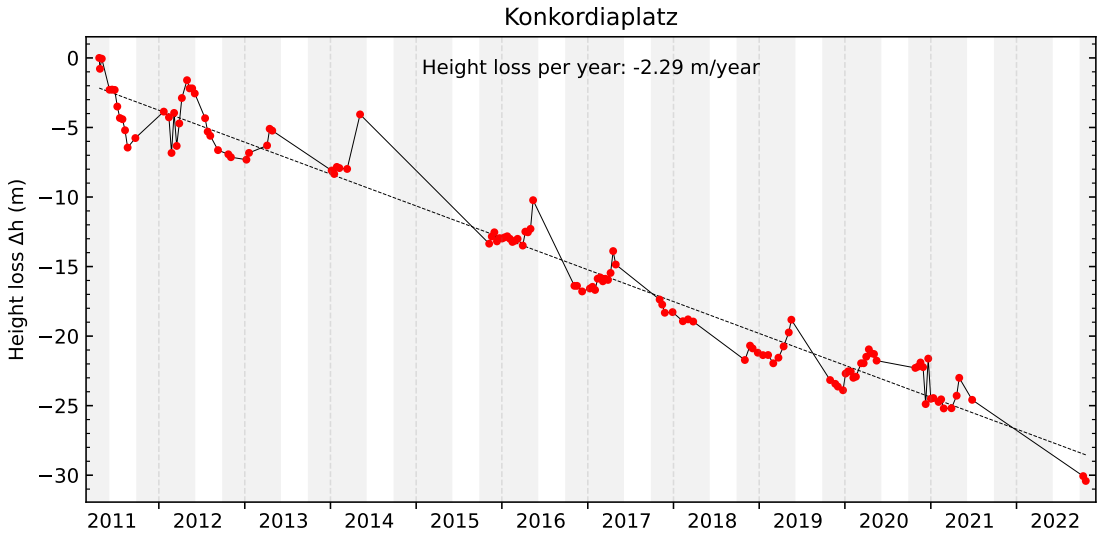

(a)

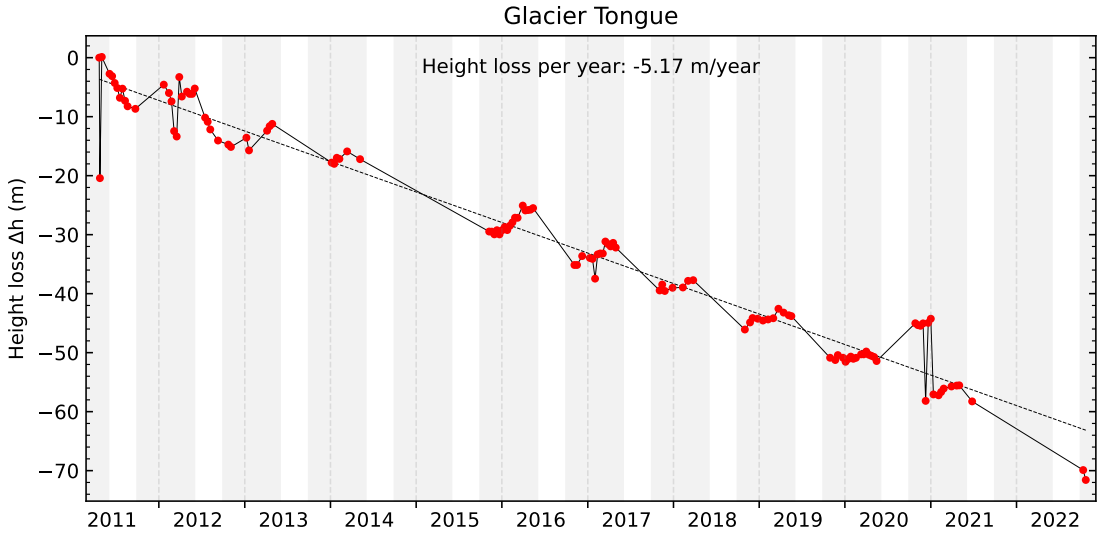

(b)

Figure 4.4: Cumulative average height loss over time (2011-2022): (a) Konkordiaplatz Area and (b) Tongue Area - (a) and (b) display the cumulative average height loss relative to the initial measurement on April 22, 2011, for the Konkordiaplatz area and the tongue area as defined in Figure 2.1. Both subfigures consist of 124 red dots, representing cumulative height loss at various timestamps between 2011 and 2022. The gray shaded region highlights the winter season from October 1 to May 31. A dashed line in each subfigure indicates the linear regression fit, with the slope coefficient providing the annual height loss rate for the respective area.

4.2.2 Elevation Loss for Two Five-Year Periods

In this subsection, we analyze elevation loss over two distinct five-year periods within the Aletsch Glacier, providing a comprehensive view of its dynamic changes. The first period, from April 22, 2011, to April 21, 2016, and the second, spanning from November 3, 2017, to October 23, 2022, allow for a comparative examination. Elevation change maps depicted in Figure 4.5 reveal that during 2011-2016, the Aletsch Glacier experienced a mean elevation loss of -6.72 meters, while for 2017-2022, the mean elevation loss amounted to -6.5 meters. Notably, only few small accumulation zones in blue signifying positive elevation changes were observed in the Aletsch firn north faces, contrasting with the glacier tongue's substantial height loss of -40 meters, highlighted in red.

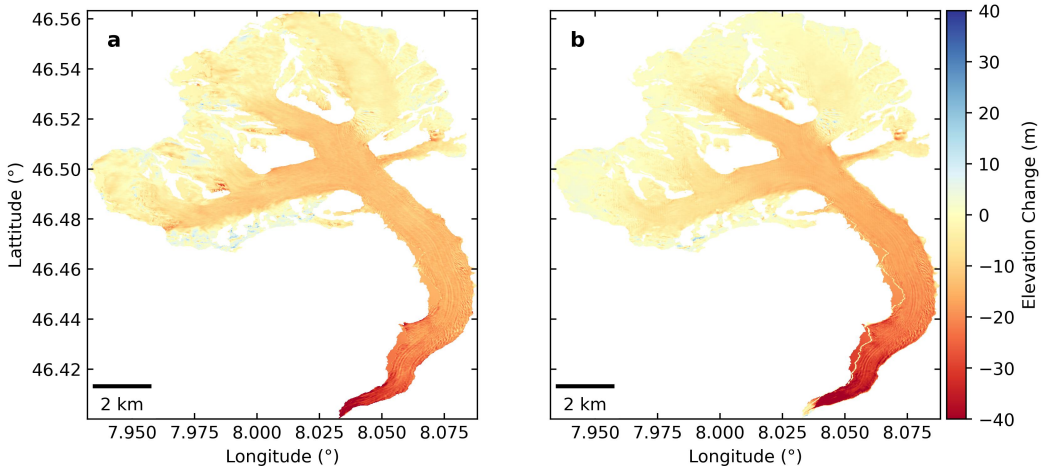

Figure 4.5: Elevation change map of the Great Aletsch Glacier between 2011-2016 **a** (April 22, 2011 to April 21, 2016) and between 2017-2022 **b** (November 3, 2017 to October 23, 2022). The colormap shows the negative elevation changes in red and the positive elevation changes in blue. The glacier outline was selected from GLAMOS [2]. Coordinate Reference System (CRS): Latitude (°)/Longitude (°) in World Geodetic System 1984 (WGS 84).

Figure 4.6 further provides a 3D view of the glacier and its mean annual height changes, showing that the mean annual height change was $-1.34\ \mathrm{m\,a^{-1}}$ during the period 2011-2016 and $-1.32\ \mathrm{m\,a^{-1}}$ in the more recent period, with heightened maximum values of $-9.25\ \mathrm{m\,a^{-1}}$and $-11.60\ \mathrm{m\,a^{-1}}$, respectively.
Figure 4.7 highlights the elevation-dependent annual height loss for the two periods 2011-2016 and 2017-2022. To obtain these elevation-dependent height change profiles for the Great Aletsch Glacier, we utilized the swissALTI3D DEM to generate masks of the glacier, each spanning a 10-meter difference in elevation, starting from 1700 meters and extending up to 4000 meters. For example, mask1 covered the elevation range of 1700-1710 meters, mask2 encompassed 1710-1720 meters, and so on. Within each of these masks, we calculated the mean height change and its corresponding standard deviation of the dDEM. The results for the period 2017-2022 reveal a distinct elevation-dependent pattern, with a steeper slope between 1900 and 2700 meters, indicating greater height loss. Below 1900 meters, where the glacier has retreated, there is no longer any ice, resulting in a peak reaching zero.

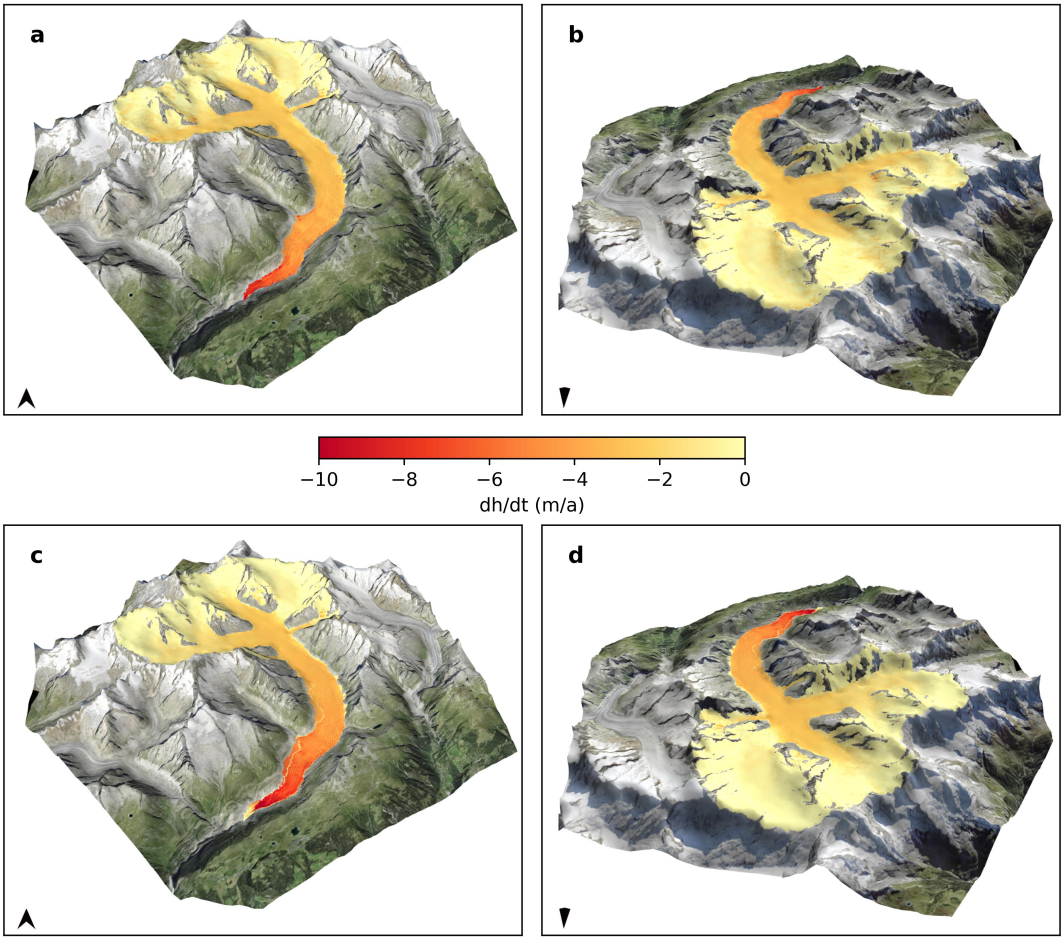

Figure 4.6: 3D representation of the Aletsch Glacier overlaid with the mean annual height change (dh/dt) for two different periods. **a** and **b** depict the mean dh/dt for the period 2011-2016 (April 22, 2011 to April 21, 2016), while **c** and **d** represent the period 2017-2022 (November 3, 2017 to October 23, 2022). **a** and **c** provide a perspective looking north, while **b** and **d** offer a view looking south.

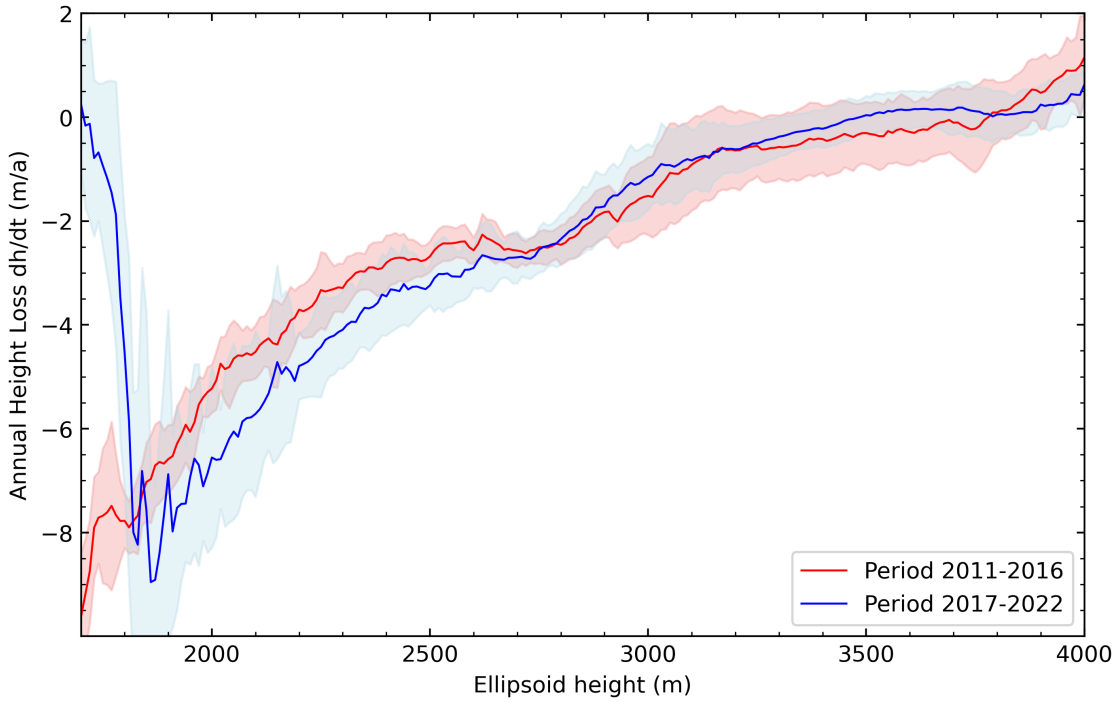

Figure 4.7: Elevation-dependant heigth loss of the Great Aletsch Glcaier for the period 2011-2016 (April 22, 2011 to April 21, 2016) red solid line and the period 2017-2022 (November 3, 2017 to October 23, 2022) blue solid line. Shaded regions in corresponding colors indicate the standard deviation for each period.

Chapter 5

Discussion

5.1 Validation and Comparison of DEMs

In Section 4.1, we observed that TanDEM-X heights were consistently 4.7 meters below GPS heights. This difference can be attributed to several factors, including the inherent characteristics of microwave penetration, which tend to increase at higher elevations, see Figure 4.1. The microwave penetration phenomenon is supported by field measurements taken during dry snow conditions, indicating the occurrence of penetration, as discussed in the Article [9]. These results highlight the importance of considering microwave penetration effects when comparing different DEM from different season. Moreover, the comparison between our DEM generation method and another approach revealed in Figure 4.2 a mean difference of 0.52 meters with a standard deviation of 3.13 meters. These variations can be attributed to the specific techniques and algorithms employed in each method. Notably, these differences may affect the accuracy of the elevation data and should be taken into account when interpreting glacier height loss.

5.2 Elevation Loss of the Great Aletsch Glacier

Our investigation into elevation changes over time has unveiled distinct trends within various regions of the Aletsch Glacier. Each region exhibits marked seasonal variability, characterized by a rise in elevation during the winter months and a subsequent decline during the summer season. Through the utilization of linear regression models, we have quantified the annual rates of elevation loss for key areas within the glacier. Specifically, we have determined an average loss of approximately $-1.01\ \mathrm{m\,a^{-1}}$ for the Aletsch Glacier as a whole, $-2.3\ \mathrm{m\,a^{-1}}$ for Konkordiaplatz, and a more substantial $-5.2\ \mathrm{m\,a^{-1}}$ for the Glacier Tongue. These figures underline the substantial variability in glacier behavior, with the Glacier Tongue experiencing the most rapid decline in elevation. This disparity is likely attributable to its lower elevation and increased exposure to elevated temperatures. It is noteworthy that our analysis was hampered by a lack of data for the winters of 2014-2015 and 2021-2022. Nonetheless, thanks to the linear regression model, we can regard the effects of varying penetration depths, seasonal height fluctuations, and the lack of data for two winters as negligible. However, for further refinement, it may be advisable to exclude data from the two summer seasons to mitigate the influence of seasonal fluctuations.
When assessing the trends in elevation loss over two consecutive five-year periods, specifically from 2011 to 2016 and 2017 to 2022, we observed a relatively consistent rate of loss.

During the first period, the average rate of loss was approximately $-1.34\,\mathrm{m\,a^{-1}}$, and during the second period, it was $-1.32\,\mathrm{m\,a^{-1}}$. Nevertheless, it is crucial to point out that, with regard to the elevation-dependent metric, we identified a higher annual elevation loss during the latter period (2017-2022) below the 2700-meter elevation threshold. Additionally, it is important to note that our initial Digital Elevation Model (DEM) difference corresponds to the end of the winter season, while in the period from 2017 to 2022, the DEM difference is determined at the end of the winter season due to the unavailability of TanDEM-X data beyond October 10, 2023.

5.3 Limitations of our Study for Glacier Mass Loss Calculation

Our study is not without limitations, which must be considered when estimating glacier mass loss. Firstly, we employed the same glacier outline in 2017 for the entire study period from 2011 to 2022 to calculate the volume loss. Given that glacier outlines evolve over time due to glacier recession, obtaining yearly glacier outlines should enhance the accuracy of mass loss calculations. Additionally, we maintained the same ice density throughout the calculation of glacier mass loss.
Furthermore, it's worth noting that a significant portion of our study area relies on interpolation within the glacier outlines, amounting to approximately 14% of the total surface area. This interpolation introduces a level of uncertainty into our calculations.

Chapter 6

Conclusion

In conclusion, in this study we have presented a comprehensive analysis of the recent height changes of the Great Aletsch Glacier using TanDEM-X time series data spanning from 2011 to 2022.
To generate high-resolution DEMs of the Aletsch Glacier using TanDEM-X time series data we used an iterative approach to update the reference DEM using differential interferometry.
The resulting DEMs were validated against GPS measurements and showed a good agreement with a mean error of -4.3 m, which was attributed to the microwave penetration depth into dry snow.
We used a local hypsometric interpolation to fill the data gaps inside the glacier outline of the dDEMs. The dDEMs were used to estimate the elevation and mass changes of the glacier over the study period, as well as the spatial and temporal variations of these changes.
The main findings of this study are:

- The Aletsch Glacier has experienced a significant elevation loss of $-1.01\ \mathrm{m\,a^{-1}}$ on average, with higher rates at lower elevations and near the glacier tongue.
- The Konkordiaplatz area has an average elevation loss of $-2.3\ \mathrm{m\,a^{-1}}$, while the Glacier Tongue has $-5.2\ \mathrm{m\,a^{-1}}$.
- The elevation loss has accelerated in the last five years (2017-2022) compared to the previous five years (2011-2016) below 2700 m.
- The mass loss of the glacier was estimated to be $-68\ \mathrm{Mt\,a^{-1}}$ on average.

With the potential of TanDEM-X data, we have revealed the height changes of the Great Aletsch Glacier at high spatial and temporal resolutions, and provided valuable insights into the glacier response to the ongoing climate change. However, this study also has some limitations that need to be considered in future work, such as:

- The estimation of the microwave penetration depth and its spatial and temporal variations, which could improve the accuracy of the DEMs and reduce the systematic bias.

- The reduction of the interpolated area inside the glacier, which could be achieved by using more advanced techniques to deal with shadows and layover effects in SAR imagery.
- The update of the glacier outline for each year, which account for the mean elevation and mass loss calculation.
- The assumption of the same ice density for the mass loss calculation, which could introduce uncertainties and errors in the estimation of glacier mass change.

Appendix A

Appendix

A.1 Key Characteristics of the Glacier Outline

Table A.1: Key Characteristics of the Glacier Outline

Characteristic	**Value**
Year of Aerial Image Acquisition	2017
Area	78.48 km^2
Length	23.54 km
Elevation Range	
Minimum	1605 m a.s.l
Mean	3051 m a.s.l
Maximum	4120 m a.s.l
Average Slope (degree)	15.68°
Average Aspect (degree)	142°

A.2 Key Characteristics of Konkordiaplatz and the Glacier Tongue Region

Table A.2: Key Characteristics of Konkordiaplatz and the Glacier Tongue

Characteristic	**Konkordiaplatz**	**Glacier Tongue**
Area	7.38 km^2	1.63 km^2
Elevation Range		
Minimum	2600 m a.e	1900 m a.e
Mean	2724 m a.e	1895 m a.e
Maximum	2800 m a.e	2100 m a.e
Average Slope (degree)	5.56°	9.61°
Average Aspect (degree)	132°	201°

A.3 Specification of the TanDEM-X SAR Data Acquisition

Table A.3: Baseline and Height of Ambiguity in meters for TanDEM-X Data from 2011-04-22 to 2018-12-26

Date	Baseline (m)	HOA (m)	Date	Baseline (m)	HOA (m)
2011-04-22	42.43	114.08	2015-12-11	25.43	190.63
2011-04-25	151.48	25.10	2015-12-22	25.02	193.20
2011-05-03	41.87	115.68	2016-01-02	24.88	194.83
2011-06-05	35.12	137.72	2016-01-13	31.93	150.52
2011-06-16	33.24	145.69	2016-01-24	31.73	152.04
2011-06-27	29.23	165.98	2016-02-04	32.50	148.60
2011-07-08	26.44	184.85	2016-02-15	129.36	37.24
2011-07-19	24.64	198.50	2016-02-26	139.62	34.55
2011-07-30	21.03	234.74	2016-03-08	148.93	32.33
2011-08-10	19.60	254.74	2016-03-30	167.04	28.87
2011-08-21	18.72	268.09	2016-04-10	177.02	27.27
2011-09-23	17.29	296.12	2016-04-21	187.15	25.79
2012-01-22	11.38	-449.86	2016-05-02	196.60	24.57
2012-02-02	11.58	-441.38	2016-05-13	206.41	23.40
2012-02-13	11.09	-462.92	2016-11-05	10.28	577.38
2012-02-24	10.82	-475.79	2016-11-16	10.69	543.05
2012-03-06	10.24	-504.48	2016-12-08	11.27	501.24
2012-03-17	10.02	-512.84	2017-01-10	10.34	571.49
2012-03-28	10.32	-500.45	2017-01-21	10.50	557.37
2012-04-08	66.15	72.64	2017-02-01	10.49	561.09
2012-04-30	65.40	73.42	2017-02-12	85.98	56.22
2012-05-11	67.00	71.84	2017-02-23	82.42	58.62
2012-05-22	66.12	72.65	2017-03-06	64.85	74.58
2012-06-02	66.30	72.58	2017-03-17	57.27	84.49
2012-07-16	64.73	74.42	2017-03-28	53.83	90.09
2012-07-27	61.95	77.55	2017-04-08	49.57	97.68
2012-08-07	60.65	79.21	2017-04-19	44.01	110.25
2012-09-09	57.39	83.70	2017-04-30	31.25	156.32
2012-10-23	46.11	104.60	2017-11-03	219.92	22.13
2012-11-03	43.98	109.63	2017-11-14	210.24	-23.16
2013-01-08	14.61	-435.56	2017-11-25	200.91	-24.25
2013-01-19	13.85	-487.34	2017-12-28	129.79	37.49
2013-01-30	16.62	-345.25	2018-02-10	115.36	-42.22
2013-04-06	78.98	61.28	2018-03-04	103.52	47.06
2013-04-17	59.73	80.96	2018-03-26	96.78	-50.39
2013-04-28	36.50	132.57	2018-11-01	89.62	-54.45
2015-11-08	18.23	267.16	2018-11-23	219.29	-22.17
2015-11-19	27.13	178.67	2018-12-04	214.81	22.60
2015-11-30	25.16	192.13	2018-12-26	160.91	-30.23

Table A.4: Baseline and Height of Ambiguity in meters for TanDEM-X Data from 2019-01-17 to 2022-10-23

Date	Baseline (m)	HOA (m)
2019-01-17	151.99	-32.01
2019-02-08	138.07	35.24
2019-03-02	128.85	-37.79
2019-03-24	120.08	40.54
2019-04-15	111.38	43.74
2019-05-07	194.48	-25.01
2019-05-18	190.94	25.44
2019-10-30	146.47	33.20
2019-11-21	138.01	35.26
2019-12-02	133.11	36.56
2019-12-24	116.87	41.68
2020-01-04	111.90	-43.54
2020-01-15	106.53	45.73
2020-01-26	101.74	47.91
2020-02-06	96.68	-50.45
2020-02-17	92.57	52.71
2020-03-10	95.86	-50.86
2020-03-21	99.67	-48.91
2020-04-01	103.41	47.13
2020-04-12	107.41	45.36
2020-04-23	112.86	-43.16
2020-05-04	126.34	-38.52
2020-05-15	137.53	35.35
2020-10-27	193.80	25.10
2020-11-07	189.67	25.65
2020-11-18	185.68	26.20
2020-11-29	182.73	-26.64
2020-12-10	179.87	-27.07
2020-12-21	175.35	-27.77
2021-01-01	176.11	27.63
2021-01-12	173.53	-28.06
2021-02-03	169.96	28.63
2021-02-14	168.04	-28.98
2021-02-25	160.86	-30.29
2021-03-30	154.28	31.57
2021-04-21	150.36	-32.41
2021-05-02	143.19	34.04
2021-06-26	120.21	-40.51
2022-10-12	107.47	45.36
2022-10-23	110.61	44.03

A.4 dDEM Generation Workflow

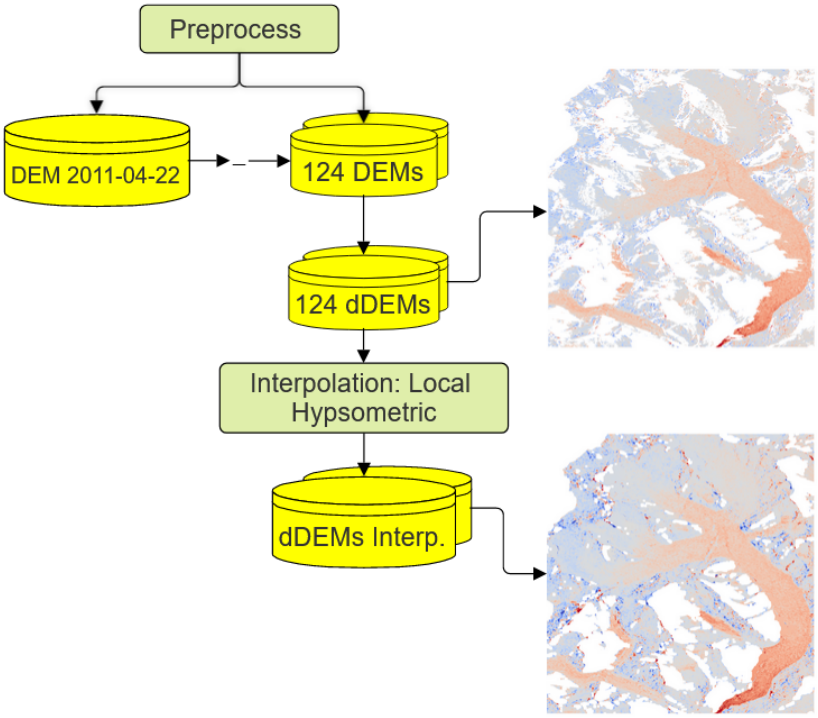

Figure A.1: Workflow for dDEM generation with example of dDEM at top right and dDEM interpolated at bottom right.

A.5 Characterisctics of Interpolated dDEMs

The Tables below show the number of pixels interpolated for the three zones defined in Section 2.1 and 2.2. The total number of pixels for the Great Altesch Glacier, Konkordiaplatz and the Tongue zones are respectively 706984, 66433 and 14696.

Table A.5: Surface interpolated in the DEMs from 2011-04-22 to 2014-01-28 for the three zones: The Great Aletsch Glacier, Konkordiaplatz and the Glacier Tongue.

	Number of Pixel Interpolated			Surface Interpolated (%)		
End Date	Glacier	Konkordiaplatz	Tongue	Glacier	Konkordiaplatz	Tongue
2011-04-22	0	0	0	0	0	0
2011-04-25	286579	8365	4406	41	13	30
2011-05-03	94486	1456	1737	13	2	12
2011-06-05	97340	1253	1641	14	2	11
2011-06-16	97132	1203	1615	14	2	11
2011-06-27	95745	1177	1651	14	2	11
2011-07-08	97758	1175	1569	14	2	11
2011-07-19	92933	1144	1781	13	2	12
2011-07-30	100675	1119	1638	14	2	11
2011-08-10	101020	1176	1716	14	2	12
2011-08-21	103733	1175	1738	15	2	12
2011-09-23	100654	1187	1707	14	2	12
2012-01-22	117866	2762	3571	17	4	24
2012-02-13	117344	2712	4006	17	4	27
2012-02-24	132012	2233	3487	19	3	24
2012-03-06	112686	2919	2916	16	4	20
2012-03-17	112406	2296	2723	16	3	19
2012-03-28	130820	2506	4323	19	4	29
2012-04-08	94120	1325	1780	13	2	12
2012-04-30	94958	1325	1775	13	2	12
2012-05-11	94167	1308	1770	13	2	12
2012-05-22	94167	1308	1770	13	2	12
2012-06-02	98923	1935	3653	14	3	25
2012-07-16	84763	1208	1725	12	2	12
2012-07-27	94066	1328	1780	13	2	12
2012-08-07	94161	1327	1781	13	2	12
2012-09-09	92034	1306	1761	13	2	12
2012-10-23	84644	1223	1727	12	2	12
2012-11-03	92012	1297	1759	13	2	12
2013-01-08	113364	1700	2665	16	3	18
2013-01-19	106763	2083	2643	15	3	18
2013-04-06	91949	1305	1758	13	2	12
2013-04-17	91998	1304	1758	13	2	12
2013-04-28	94899	1382	1665	13	2	11
2014-01-06	95044	1328	1777	13	2	12
2014-01-17	92462	1303	1756	13	2	12
2014-01-28	92034	1310	1761	13	2	12

Table A.6: Surface interpolated in the DEMs from 2014-02-08 to 2018-11-23 for the three zones: The Great Aletsch Glacier, Konkordiaplatz and the Glacier Tongue.

	Number of Pixel Interpolated			Surface Interpolated (%)		
End Date	Glacier	Konkordiaplatz	Tongue	Glacier	Konkordiaplatz	Tongue
2014-02-08	92521	1302	1756	13	2	12
2014-03-13	92618	1315	1763	13	2	12
2014-05-07	99791	2056	2435	14	3	17
2015-11-08	95035	1212	2066	13	2	14
2015-11-19	91993	1313	1761	13	2	12
2015-11-30	94364	1349	1793	13	2	12
2015-12-11	94341	1342	1796	13	2	12
2015-12-22	94300	1339	1794	13	2	12
2016-01-02	94375	1347	1794	13	2	12
2016-01-13	94426	1362	1795	13	2	12
2016-01-24	94480	1349	1790	13	2	12
2016-02-04	91986	1310	1762	13	2	12
2016-02-15	94257	1339	1791	13	2	12
2016-02-26	94405	1342	1800	13	2	12
2016-03-08	94445	1354	1802	13	2	12
2016-03-30	94354	1344	1794	13	2	12
2016-04-10	94433	1357	1797	13	2	12
2016-04-21	84757	1217	1729	12	2	12
2016-05-02	94383	1337	1806	13	2	12
2016-05-13	94393	1352	1801	13	2	12
2016-11-05	112082	1737	1722	16	3	12
2016-11-16	112082	1737	1722	16	3	12
2016-12-08	103675	1601	1879	15	2	13
2017-01-10	111807	1509	1722	16	2	12
2017-01-21	111602	1644	1754	16	2	12
2017-02-01	113414	1734	1928	16	3	13
2017-02-12	84673	1213	1732	12	2	12
2017-02-23	84650	1222	1726	12	2	12
2017-03-06	84584	1213	1730	12	2	12
2017-03-17	84619	1220	1726	12	2	12
2017-03-28	84602	1218	1728	12	2	12
2017-04-08	84811	1218	1731	12	2	12
2017-04-19	84617	1221	1726	12	2	12
2017-04-30	84659	1220	1727	12	2	12
2017-11-03	95800	1380	1798	14	2	12
2017-11-14	84564	1205	1730	12	2	12
2017-11-25	84561	1210	1729	12	2	12
2017-12-28	84695	1219	1726	12	2	12
2018-02-10	84484	1202	1729	12	2	12
2018-03-04	84717	1224	1728	12	2	12
2018-03-26	84663	1202	1732	12	2	12
2018-11-01	84605	1212	1728	12	2	12
2018-11-23	84570	1210	1728	12	2	12

Table A.7: Surface interpolated in the DEMs from 2018-12-04 to 2022-10-23 for the three zones: The Great Aletsch Glacier, Konkordiaplatz and the Glacier Tongue.

	Number of Pixel Interpolated			Surface Interpolated %		
End Date	Glacier	Konkordiaplatz	Tongue	Glacier	Konkordiaplatz	Tongue
2018-12-04	84629	1225	1730	12	2	12
2018-12-26	84633	1211	1728	12	2	12
2019-01-17	84551	1204	1726	12	2	12
2019-02-08	84724	1218	1727	12	2	12
2019-03-02	84491	1204	1729	12	2	12
2019-03-24	84709	1217	1727	12	2	12
2019-04-15	84694	1217	1729	12	2	12
2019-05-07	84566	1211	1723	12	2	12
2019-05-18	84659	1212	1730	12	2	12
2019-10-30	84693	1219	1724	12	2	12
2019-11-21	84677	1216	1733	12	2	12
2019-12-02	84591	1220	1728	12	2	12
2019-12-24	84706	1224	1727	12	2	12
2020-01-04	95216	1353	1806	13	2	12
2020-01-15	94357	1348	1796	13	2	12
2020-01-26	94366	1351	1794	13	2	12
2020-02-06	95306	1355	1801	13	2	12
2020-02-17	94324	1352	1797	13	2	12
2020-03-10	95225	1353	1806	13	2	12
2020-03-21	95225	1353	1806	13	2	12
2020-04-01	94272	1341	1792	13	2	12
2020-04-12	94286	1341	1798	13	2	12
2020-04-23	95196	1371	1792	13	2	12
2020-05-04	95253	1377	1795	13	2	12
2020-05-15	94284	1347	1795	13	2	12
2020-10-27	94349	1342	1800	13	2	12
2020-11-07	94251	1338	1787	13	2	12
2020-11-18	94452	1351	1795	13	2	12
2020-11-29	95154	1344	1797	13	2	12
2020-12-10	95075	1344	1801	13	2	12
2020-12-21	95168	1345	1802	13	2	12
2021-01-01	94392	1343	1805	13	2	12
2021-01-12	95242	1368	1794	13	2	12
2021-02-03	94387	1345	1795	13	2	12
2021-02-14	95121	1363	1796	13	2	12
2021-02-25	95062	1355	1796	13	2	12
2021-03-30	94411	1361	1797	13	2	12
2021-04-21	95092	1362	1794	13	2	12
2021-05-02	94376	1345	1807	13	2	12
2021-06-26	95198	1359	1805	13	2	12
2022-10-12	94370	1345	1795	13	2	12
2022-10-23	100703	1590	2989	14	2	20

Bibliography

[1] PROJ.org Datumgrid CDN. `https://cdn.proj.org/`.

[2] E. Hodel A. Bauder M. Fischer Y. Weidemann H. Bartschi A. Linsbauer, M. Huss and E. Schmassmann. The new Swiss Glacier Inventory SGI2016: From a topographical to a glaciological dataset. *Frontiers in Earth Science*, 9, 2021.

[3] Bauder, A. and Huss, M. and Linsbauer, A. The Swiss Glaciers 2019/20 and 2020/21. *Glaciological Report No. 141/142 of the Cryospheric Commission of the Swiss Academy of Sciences (SCNAT)*, page 173, 2022.

[4] A. Bauder D. Farinotti, M. Huss and M. Funk. An estimate of the glacier ice volume in the Swiss Alps. *Global and Planetary Change*, 68(3):225–231, 2009.

[5] A. Dehecq. xDEM. `https://xdem.readthedocs.io/en/stable/index.html`. Accessed: Nov. 8, 2020.

[6] Federal Office of Topography swisstopo. Rapport sur le release de la publication 2022 swissALTI3D. Technical report, Federal Office of Topography swisstopo, 2022.

[7] M. Huss. Density assumptions for converting geodetic glacier volume change to mass change. *Scientific Data*, 7:877â887, 2013.

[8] Jr. Karpilo, R. D. Glacier Monitoring Techniques. *Geological Society of America*, pages 141–162, 2009.

[9] S. Leinss and P. Bernhard. TanDEM-X: Deriving InSAR Height Changes and Velocity Dynamics of Great Aletsch Glacier. *IEEE Journal of Selected Topics in Applied Earth Observations and Remote Sensing*, 14:4798–4815, 2021.

[10] Federal Office of Topography swisstopo. swissALTI3D. `https://www.swisstopo.admin.ch/en/geodata/height/alti3d.html`.

[11] Federal Office of Topography swisstopo. Le modèle de terrain à haute résolution de la Suisse: swissALTI3D. Technical report, Federal Office of Topography swisstopo, 2022.

[12] P. Rizzoli et al. Generation and performance assessment of the global TanDEM-X digital elevation model. *ISPRS J. Photogramm. Remote Sens.*, 132:119–139, 2017.

[13] C. Rossi T. Fritz S. Duque, U. Balss and W. Balzer. CoSSC Generation and Interferometric Considerations. *TD-PGS-TN-3129*, 2012.

[14] GAMMA Remote Sensing. Differential Interferometry and Geocoding Software. Technical report, 2015.

[15] G. Krieger T. Fritz, B. Brautigam and M. Zink. TanDEM-X Ground Segment - TanDEM-X Experimental Product Description. *TD-PGS-TN-3129*, 2012.

[16] UNESCO World Heritage Centre. Swiss Alps Jungfrau-Aletsch. `https://whc.unesco.org/en/list/1037`.

[17] S. Vijay and M. Braun. Seasonal and interannual variability of Columbia Glacier, Alaska (2011 2016): Ice velocity, mass flux, surface elevation and front position. *Remote Sensing*, 9:1–18, 2017.

Eidgenössische Technische Hochschule Zürich
Swiss Federal Institute of Technology Zurich

Chair of Earth Observation and Remote Sensing
Prof. Dr. I. Hajnsek

Title of work:

Revealing the Recent Height Changes of the Great Altesch Glacier Using TanDEM-X DEM Series

Thesis type and date:

Master Thesis, October 2023

Supervision:

Shiyi Li
Prof. Dr. Irena Hajnsek

Student:

Name:	Pierre-Louis Vlieghe
E-mail:	pvlieghe@student.ethz.ch
Legi-Nr.:	17-813-437
Semester:	5

Statement regarding plagiarism:

By signing this statement, I affirm that I have read and signed the Declaration of Originality, independently produced this paper, and adhered to the general practice of source citation in this subject-area.

Declaration of Originality:

`http://www.ethz.ch/faculty/exams/plagiarism/confirmation_en.pdf`

Zurich, 20. 10. 2023: _____